Agglomeration of Pt thin films on dielectric substrates

H. Galinski,* T. Ryll, P. Elser, J. L. M. Rupp, A. Bieberle-Hütter, and L. J. Gauckler
Nonmetallic Inorganic Materials, Department of Materials, ETH Zurich, Zurich, Switzerland
(Received 10 August 2010; revised manuscript received 21 October 2010; published 9 December 2010)

The agglomeration of metal thin films on dielectric materials is a topic of high technological importance. In this contribution, a coupled morphology-agglomeration approach has been chosen to reveal the basic mechanism of rupture, mass transport, and the substrate dependence of agglomeration. The morphological evolution of Pt thin films has been investigated by means of scanning electron microscopy, atomic force microscopy, and focused ion-beam (FIB) etching techniques. Pt thin films were deposited on amorphous Si_3N_4 and polycrystalline yttria stabilized ZrO_2 substrates and subjected to heat treatments up to 1193 K for 2 h. Three main observations have been made: (i) the early stage of rupture can be described via basic thermodynamics as an order-disorder transition. The dominating mechanism of initial film rupture is a defect associated barrierless nucleation of holes in the spinodal regime of the Pt thin film as shown by means of Minkowski measures. (ii) Up to 1073 K the hole growth is found to be a surface-diffusion limited process, and in first approximation it is in agreement with Brandon and Bradshaw's theory for the morphological evolution of thin metal films at elevated temperatures. Values for mass transport have been derived. (iii) It is shown that two in general independent physical processes control the morphological evolution and kinetics of thin-film agglomeration: one attributes to the film-ambient interface and the other to the film-substrate interface. Void formation at the film-substrate interface is enhanced by a factor of 9 in the case of the amorphous-crystalline interface due to a lower adhesion energy of the film. The corresponding adhesion energies have been determined experimentally using FIB techniques and the Wulff-Kaishew theorem for equilibrium crystal shapes.

DOI: 10.1103/PhysRevB.82.235415 PACS number(s): 68.60.Dv, 68.35.Md, 68.55.J−, 81.07.−b

I. INTRODUCTION

Agglomeration of metal thin films on dielectric materials has been a research topic since years[1] and is of intense relevance in the field of integrated circuits[2,3] and electrode engineering for microsolid oxide fuel cells.[4] The interest is not only motivated by industrial needs of new dielectric substrates for further miniaturization of semiconductor devices but also by fundamental interests in the physical properties of discontinuous thin films that are formed in the presence of an heterophase interface.[5,6] In general, metals and dielectric materials possess distinct diametric bonding characteristics.[7] The morphological stability of a metal thin film on a dielectric material is thus conditioned by the aspect ratio, the interaction across the interface,[8] and the tendency of the thin film to reduce its free surface energy. In the case of a weak interaction between the film and the substrate the minimization of the total Gibbs free energy gives rise to decomposition and agglomeration of thin metallic films. Thin-film agglomeration has been subjected to research under several aspects: thermodynamics and kinetics,[5,9–13] mass transport via surface diffusion,[14–17] impact of surface energy anisotropies,[13,18] fingering instabilities,[6,19,20] Ostwald ripening of islands,[21] hole pattern,[22] and hillock formation.[23,24] Most of the fundamental theoretical work has been carried out by Srolovitz and Safran since the publication of the well-known paper of Brandon and Bradshaw.[14] Srolovitz and Safran developed a complete stability theory for thin films covering kinetics[10] and energetics.[9] Based on their proposed stability criterion[9] for grain boundary grooves and triple junctions Genin and Mullins derived an analytical solution for hole formation in the vicinity of a triple junction[11] and subsequently showed its validity under experimental conditions.[12] Based on agglomeration experiments of thin-metal lines, Jiran and Thompson elaborated the model of Brandon and Bradshaw for the retraction of the film at the line's edges, so-called fingering instabilities.[6,19] Wong *et al.*[25–28] examined numerically the linear stability of several edge configurations as a function of different contact angles. Recently, Kan[20] presented a numerical solution for the evolving perturbation at the line's edge in three dimensions. Theoretical attention has been drawn as well on the influence of surface energy anisotropies on the physics of agglomeration.[13,18] Theoretical evidence has been presented that anisotropies of the surface energy postpone the onset of agglomeration but the value and speed of the agglomeration stays unaffected.[18] In a recent contribution, Thiele *et al.*[29] showed that film rupture by nucleation exists in the spinodal regime. By analyzing the final agglomeration pattern, it is thus possible to distinguish between instability-dominated agglomeration and nucleation-dominated agglomeration within the linearly unstable range.[29–31] Although there are several experimental contributions on the physics of thin-film agglomeration,[16,17,21–24] to our knowledge, there is no experimental data available that attributes directly to the substrate influences on the physics of thin-film agglomeration.

The main objective of this paper is to establish a relation between the observable macroscopical changes in the morphology of the thin film with its underlying agglomeration kinetics and configurational forces. The investigation will focus on how the presence of interfaces affects the mechanism of rupture and the operative transport mechanism which finally determines the equilibrium morphology of the thin film.[5] Therefore traditional morphological measures such as surface coverage have been chosen alongside more sophisticated surface descriptors such as the Minkowski functionals,

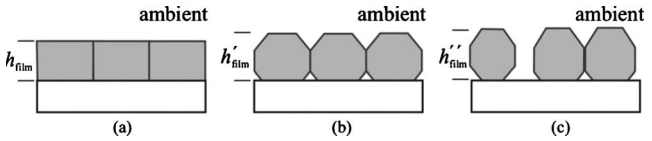

FIG. 1. ($h_{film} < h'_{film} < h''_{film}$) Schematic description of thin-film agglomeration of a dense thin film (a). Temperature treatment leads to grain-boundary grooving at both interfaces (b) triggered by the chemical potential difference in the film, grooves are enlarged by diffusion and form holes (c).

which are successfully used to analyze dewetting phenomena of liquid metal and polymer thin films.[32–34]

In the present study, amorphous silicon nitride grown on silicon (Si_3N_4/Si) and polycrystalline yttria stabilized zirconium oxide (ZrO_2) have been chosen as model metal/dielectric systems in order to study thin-film agglomeration. These two systems possess distinct diametric bonding characteristics in form of a crystalline/amorphous (ca) and a crystalline/crystalline (cc) interface. Recently developed thermodynamic models of metal/oxide interfaces[35] and the thermodynamics of solid-state amorphization[36] show that the interfacial energy of a crystalline metal on an amorphous substrate is generally smaller than in the case of a crystalline substrate. This difference condensates in a formulation of the system's total free energy.[37] In equivalence to Au/ZrO_2 (Ref. 38) the Pt/ZrO_2 interface can be regarded as semicoherent[39] due to a lattice-parameter misfit $f=[(a_f-a_s)/a_s]=0.23$. In contrast to the Pt/ZrO_2 system, the Pt/Si_3N_4 interface is incoherent.

This paper is structured as follows: Sec. II derives the basic thermodynamical and kinetical models necessary to describe the morphology evolution. A phenomenological approach describing thin-film agglomeration as order-disorder transition, is followed by the introduction of Minkowski functionals as a tool for describing morphologies, the Brandon-Bradshaw model[14] to determine the operative mass transport via hole growth and the Wulff-Kaishew theorem to evaluate the interfacial energies. In Sec. IV detailed results on thin-film agglomeration and its convolution with the nature of the present interfaces are presented. The final section encompasses a summary of the findings and conclusions.

II. THEORETICAL BACKGROUND

A. Basics

During deposition of metal thin films via sputtering, the kinetic energy E_{kin} of the deposited atoms generally exceeds their thermal energy E_{ther}. For the deposited film, this results in a metastable configuration that tends to equilibrate, once subjected to temperature by annealing, Joule's heating or radiation. The process of equilibration manifests in the evolution of the film morphology as shown schematically in Fig. 1. It is defined by the minimization of the system's free energy F. The difference of the free energy per unit area between a dense and agglomerated thin film can be formulated as

$$\Delta F = \Delta\gamma_{fs} + \Delta\gamma_{fa} + \lambda(\gamma_{sa} - \gamma_{fs} - \gamma_{fa}). \tag{1}$$

The indexes (fs, fa, sa) correspond to the film-substrate, film-ambient, and substrate-ambient interface, respectively. $\Delta\gamma_{fs} = \gamma_{fs}^{dense} - \gamma_{fs}^{agglom.}$ denotes the difference of the interfacial energies at the inner fs interface. The same applies for $\Delta\gamma_{as}$ at the fa interface. λ stands for the uncovered area. For $\Delta F < 0$ for a given temperature T, the integrity of the thin film is no longer conserved and an agglomerated state is more favorable. If F corresponds to a double-well potential in the early stage of agglomeration, there exists for each film thickness h a critical temperature T_c. In its vicinity the transition from a continuous to a discontinuous film can be treated phenomenologically as a phase transition depending solely on one order parameter ξ. According to the work of Novick-Cohen[40] and Thiele[29] on film rupture by nucleation in the spinodal regime, we use the ansatz of Landau[41] for the free energy of a second-order transition, F reads

$$F(T,\xi) = F_0(T) + \frac{\alpha(T)(T_c - T)}{2}\xi^2 + \frac{\beta(T)}{4}\xi^4, \tag{2}$$

where α and β are temperature-dependent parameters of the system. In equilibrium $\tilde{F} = \min F(\xi)$ and the minima of the double-well potential are at

$$\xi = \sqrt{\frac{\alpha(T_c - T)}{\beta}}. \tag{3}$$

Providing that the observed and measured morphologies are equilibrium structures, the uncovered area λ is considered equal to the order parameter ξ of the system ($\lambda \equiv \xi$). The variation in F with respect to λ, defines the chemical potential of the system,

$$\frac{\partial F}{\partial \lambda} = \mu. \tag{4}$$

Following this approach, the continuous-discontinuous transition as function of the critical parameter and its scaling behavior is reproduced. This ansatz deems justified as long as the impact of the convoluted mechanisms, such as adhesion, recrystallization, tensile stresses, and hillock formation is unclear. The nature of the film-substrate interface can be treated in analogy to Jeurgens *et al.*[35,37] by different contributions to the interfacial energy. For a ca interface the film-substrate interfacial energy γ_{fs} is

$$\gamma_{fs}^{ca} = \gamma^{interaction} + \gamma^{entropy} + \gamma^{enthalpy}, \tag{5}$$

whereby $\gamma^{interaction}$, $\gamma^{entropy}$ are negative contributions due to repulsive interactions across the interface and enlarged entropy due to the disorder introduced by the incoherence of the interfaces. The enthalpy term contributes to an enthalpy increase in the metal thin film due to liquid bonding at the interface.[35] As observed for other systems (i.e., Cu/Si_3N_4) dislocation core spreading might be an additional weakening contribution on the interaction term.[42] The interfacial energy of a cc interface

$$\gamma_{fs}^{cc} = \tilde{\gamma}^{interaction} + \tilde{\gamma}^{mismatch} \tag{6}$$

consists of two terms, an interactive one that triggers the adhesion which is predominately defined by the electronic structures of film and substrate and a mismatch term that

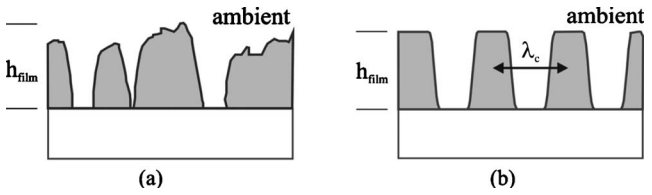

FIG. 2. Illustration of two possible agglomeration regimes (a) formation of a aperiodic hole pattern via nucleation at randomly distributed defects and (b) formation of periodic hole pattern due to spinodal dewetting with a continuous distribution of heights.

accounts for arising stresses due to the incompatibility of the two lattices.

B. Mechanisms of rupture

Two basic mechanisms of thin-film rupture are known:[10,29,30] randomly distributed formation of holes associated to microstructural defects or "spinodal dewetting" a long wave instability[31] due to thermal fluctuations which lead to a periodic spatial pattern that is highly nonstatistical (Fig. 2). Regarding the path breaking stability theory for thin films developed by Srolovitz and Safran[9,10] the rupture mechanism of nanocrystalline thin films is dominated by heterogeneously nucleating nonlinear perturbations. These perturbations are associated with nucleation barrierless defects such as triple junctions and grain-boundary grooves, whereas the triple junctions influence the film integrity more severly.[10] In contrast to the long wave instability of spinodal dewetting,[31] the perturbations in nanocrystalline thin films are localized, uncorrelated, and influence their surrounding only on a short range.[10] Theoretical evidence has been presented by Thiele and Novick-Cohen that the process of defect-dominated agglomeration can be treated as nucleation in the spinodal regime.[29,40] Furthermore a smooth transition between the periodically structured spinodal dewetting and the randomly formation of holes is postulated.[30,40] Hence, by analyzing the final agglomeration pattern the dominating mechanism of rupture can be determined.[29,30]

In contrast to common descriptors for spatial structures such as the pair-correlation function $g(r)$, the Minkowski functionals are capable to detect spatial correlations of the film geometry. They are thus suitable for testing surface morphologies on their stochastical behavior.[32–34] In two-dimensions, the three Minkowski functionals correspond to three basic morphological characteristics of the distribution of matter. These are the covered area m_1, the boundary length m_2, and the difference between the number of holes and the number of connected components, short the Euler number, m_3.[43]

Assuming that the interaction between the centers of local perturbations (i.e., triple junctions) can be neglected (e.g., the distance between two perturbation sites is large and uncorrelated from others), the associated hole formation is independent. According to the central limit theorem of probability every sum of many independent random variables tends to a normal distribution. In the case of systems with spatial extension this concept can be applied to scalar field variables (i.e., film height h) which follow multivariate Gaussian distributions such as a Gaussian random field.[44] This concept has been applied successfully to various physical problems such as rough metallic surfaces,[45] dewetting of polymer films, percolating systems, and cosmic background radiation and is, in particular, tractable as the Minkowski functionals have a unique analytical form for Gaussian random fields, where

$$m_0(h) = \frac{1}{2}\left[1 - \mathrm{erf}\left(\frac{h}{\sqrt{2}\sigma}\right)\right], \tag{7a}$$

$$m_1(h) = \frac{k}{\sqrt{8\pi}}\exp\left(-\frac{h^2}{2\sigma^2}\right), \tag{7b}$$

$$m_2(h) = \frac{hk^2}{\sqrt{2\pi^3\sigma^2}}\exp\left(\frac{h^2}{2\sigma^2}\right). \tag{7c}$$

h denotes the height, σ the variance, whereas σ^2 is the film's roughness, and k corresponds to the second derivative of the covariance in 0. For the sake of simplicity, effective measures for $s(h), u(h), \kappa(h)$ can be defined,[31,43,46] whereby

$$s(h) = s_0, \tag{8a}$$

$$u(h) = u_0 + u_2 h^2, \tag{8b}$$

$$\kappa(h) = \kappa_1 h. \tag{8c}$$

This definition is beneficial as the effective measures for Gaussian random field relate to a constant $s(h)$, a line $u(h)$, and a parabola $\kappa(h)$ which can be easily compared to experimental findings.

C. Hole growth via surface-limited diffusion

As introduced before, thin-film agglomeration is driven by the minimization of the system's free energy F [Eq. (4)], which manifests in a reconfiguration of the thin-film's morphology. The reconfiguration is accomplished by mass transport that is enhanced at surface regions of maximal curvature. The regions of maximal curvature coincide with the triple junctions of the thin film (i.e., lines where three grain boundaries meet).[11,12,47] This concept was first introduced by Mullins[11,48] for thermal grooving and thermal pinning at grain boundaries and was later extended by Brandon and Bradshaw[14] to describe the decomposition of a homogeneous crystalline surface via hole growth. In the stability theory of Srolovitz and Safran the concept has been generalized,[9,10] the static nucleation barrierless defects are regarded as local centers of perturbation. Depending on the initial amplitude the dynamic evolution of the perturbation leads to an intersection between the substrate and the surface and forms a hole.[10] Considering only surface diffusion contributing to the mass transport, one can describe the increase in chemical potential μ per atom as function of the surface's curvature K,

$$\mu(K) = K\gamma_s\Omega, \tag{9}$$

where Ω is the molar volume and γ the surface-free energy per unit area. The net flux $\mathbf{j}$ of diffusing atoms is defined as

the gradient of chemical potential and, hence, is associated with the gradient of curvature

$$\mathbf{j} = -\frac{D_s}{k_b T} \times \text{grad}\ \mu = -\frac{D_s \gamma_s \Omega}{k_b T} \times \text{grad}\ K, \qquad (10)$$

where D_s is the mass-transport coefficient. Applied on the agglomeration of thin film via hole growth it can be shown, that the time evolution of the mean hole radius $\langle r \rangle$ is equal to a product of surface mass transport coefficient D_s and kinetic parameters of the film,[14]

$$\partial_t \langle r(t,T,h) \rangle = \left(\frac{2}{5}\right)^{1/3} \pi^{1/5} \left(\frac{D_s t \gamma_s \nu \omega^2}{h^{3/2} k_b T}\right)^{-2/5} \times t^{-1}. \qquad (11)$$

Thereby ν is the surface density of sites, the other parameters have the same meaning as in the previous equations. A detailed derivation and discussion of the boundary conditions of the Brandon-Bradshaw model can be found in the Appendix of this contribution including a comparison of the experimental data set with the predictions of the Brandon-Bradshaw and the Jiran-Thompson model. It is shown that the present data set agrees well with the predictions of the Brandon-Bradshaw model, as the mean hole radius scales as predicted with the film height $h^{-3/5}$ and characteristical rims are observed around the holes. On the contrary, the model of Jiran and Thompson indicates a height dependence of h^{-3}. For annealing temperatures $T < \frac{2}{3} T_M$, it is commonly expected that the mass transfer is due to migration and formation of adatoms and surface vacancies. In the case of self-diffusion these two fundamental steps are represented by a standard Arrhenius ansatz,

$$D_s = D_0 \times \exp[-E_a/k_b T] \qquad (12a)$$

$$= D_0 \times \exp[-(E_f + E_s)/k_b T], \qquad (12b)$$

where E_f and E_s are the enthalpy of a single adatom and the enthalpy of adatom formation, respectively.[49] The prefactor D_0 is represented by an entropic term with the entropy of migration S_s, the entropy of adatom formation S_f, and a product between the vibrational frequency ν_0 and the quadratic mean jump length l of a single adatom between two sites,

$$D_0 = \nu_0 \times l^2 \times \exp[-(S_f + S_s)/k_b]. \qquad (13)$$

D. Interfacial energies and adhesion

The impact of interfacial energy, in terms of the contact angle θ, on thin-film agglomeration has been analyzed theoretically for different types and geometries of perturbation.[10,25–28] Wong *et al.*[27] presented theoretical evidence that the interfacial energy significantly affects the stability and growth rate of an catenoidal hole. In order to determine the influence of the film-substrate interface on the agglomeration mechanism experimentally, it deems necessary to determine the adhesion energy between the film and the substrate. The most suited for this task are thin films that are already disintegrated in faceted particles. Therefore, the Wulff's theorem[50,51] which relates a crystals' minimum of free energy to its equilibrium shape is extended using the Kaishew theorem[52] to estimate the influence of the underlying substrate on the equilibrium shape of the particle. Neglecting lattice mismatches the Wulff-Kaishew equation[53] reads

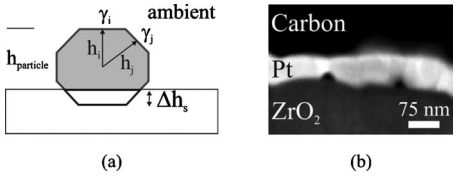

FIG. 3. (a) Schematic illustration of the Wulff-construction of an isolated particle on a random substrate and necessary measurands like the truncation depth Δh and surface energies $\gamma_{i,j}$ to determine the adhesion energy E_{ad}. (b) Cross section of a 50-nm-thick Pt film on polycrystalline ZrO_2 annealed at 923 K with grooves formed in a vicinity of a triple junction that links the surface and substrate.

$$\frac{\Delta h_s}{h_i} = \frac{E_{ad}}{\gamma_i}, \qquad (14)$$

where E_{ad} is the adhesion energy, Δh_s the truncation depth of the particle and h_i the normal distance from surface i with the surface energy γ_i to the Wulff point, see also Fig. 3(a). For increasing adhesion energies E_{ad}, the truncation of the particle will increase. If $E_{ad} = \gamma_i$, the particle will be submerged in the substrate by one half, i.e., $\Delta h_s = h_i$. By taking advantage of FIB etching techniques the truncation depth Δh_s as well as the particle shape is experimentally accessible.

III. EXPERIMENTAL

The Pt/ZrO_2 (polycrystalline) and Pt/Si_3N_4 (amorphous) systems have been selected since both of these systems show a pronounced immiscibility between the metal and insulator. Hence, it can be assumed that a chemical inert interface is formed at least at temperatures below 1273 K.[54] In order to achieve a measurement scheme of sufficient significance, Pt layers of 15–300 nm in thickness, were deposited at room temperature by magnetron sputtering ($P = 360$ W, $p_{base} = 4 \times 10^{-10}$ mbar) upon the two chosen substrates that were precleaned using isopropanol and acetone. The substrates coated with the thin platinum film were annealed in a muffel furnace for 2 h at various temperatures between 598 and 1193 K.

The morphological analysis of the samples was studied via atomic force microscopy (AFM), scanning electron microscopy (SEM), and focused ion-beam (FIB). Using a Topometrix 2000 AFM images in early stage of agglomeration were acquired and afterwards applied to the square-marching algorithm developed by Mecke *et al.*[46] to calculate the Minkowski functionals. The coverage and hole size distributions were gathered with a FESEM Leo1530 (Zeiss) equipped with a four-quadrant backscatter detector. This detector eliminates topographic information and produces a pure composition signal that is most suitable to produce binary images that can be easily be fed into common particle analysis algorithms. A reasonable systematic error for the mean hole size $\langle r \rangle$ is estimated by elongating the measured

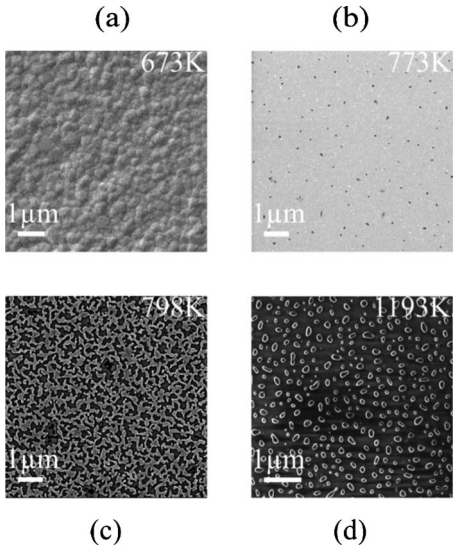

FIG. 4. SEM images of different stages of agglomeration with corresponding annealing temperature T_a of Pt on Si_3N_4 (thickness 15 nm, annealed 2 h in air). (a) 673 K ($T_a < T_c$) dense film, (b) 773 K ($T_a \geq T_c$) onset of rupture and hole formation, (c) 798 K ($T_a > T_c$) coalescences of holes, and (d) 1193 K ($T_a \gg T_c$) disintegration in separated islands.

value of $\langle r \rangle$ by two pixels. Single and multiple cross sections of the Pt/dielectric systems were cut, polished, and imaged using a Zeiss NVISION 40 FIB etching system. The stacks of multiple cross sections were aligned recursively by Stackreg[55] and reconstructed using AVS Express (Advanced Visual Systems Inc.). The voxel size of the resulting tomographic images is cubic and 11 nm in size.

IV. RESULTS AND DISCUSSION

A. Basics

For all agglomerated Pt thin films, annealed isochronically ($t=2h$) at different temperatures T_a, the expected stages[16] of film agglomeration are being reproduced for film heights h from 15 to 300 nm. In Fig. 4, the experimental stages for one set of isochronical treated samples with an initial film height of $h=15$ nm are shown representatively. For annealing temperatures T_a below a critical temperature T_c, the film surface remains coherent as shown in Fig. 4(a), i.e., the height distribution is narrow and the degree of perturbation or disorder in the film is low. Energetically speaking there is no gain in free energy $\Delta F > 0$ for these films under these conditions. Choosing annealing temperatures higher than the critical temperature $T_a \geq T_c$, the thin film undergoes a continuous-discontinuous transition indicated by holes that are formed [Fig. 4(b)] and breaking the symmetry of the original film. $\Delta F < 0$ is true. The hole density $\rho_{hole,Si_3N_4} = 0.53$ no./μm^2 and $\rho_{hole,ZrO_2} = 0.1$ no./μm^2 differs depending on the substrate material between by a factor of 5. Increasing T_a results in an enhanced hole growth accompanied by an increasing contour length until the holes start to impinge and the hole density ρ_{hole} decreases excursively as demonstrated in Fig. 4(c). In the last stage, the discontinuous film loses its percolation and an ordered array of faceted particles is formed as shown in Fig. 4(d). These particles will undergo a ripening process limited by surface diffusion, if subjected to further heat treatments as reported already earlier.[56]

In the early stages of agglomeration dominated by film rupture and hole growth, the resulting surface morphologies are similar to patterns resulting from a decomposition of binary mixtures.[57] Based on the assumption that the film rupture is dominated by nucleation in the spinodal regime,[29] the uncovered area λ is considered to be equal to the order parameter ξ of the system ($\lambda = \xi$). Note that λ solely defines the energetical changes during the continuous-discontinuous transition. In each case for the Pt/Si_3N_4 and for the Pt/ZrO_2 system two film thicknesses $h=\{15\ \text{nm}; 50\ \text{nm}\}$ have been chosen and the uncovered areas λ of the agglomerated structures have been determined via image analysis. The obtained values ξ plotted against the annealing temperature T and fitted with Eq. (3) are shown representatively for the Pt/Si_3N_4 system in Fig. 5(a). The order parameter ξ as function of T behaves highly nonlinear and has a power-law shape typical for second-order phase transitions. $\xi \approx (T_c - T)^{\epsilon}$ with $\epsilon = \frac{1}{2}$ which is consistent with the Landau theory. For early stages of agglomeration, the Landau ansatz covers sufficiently the evolution of ξ, the large errors are attributed to thermal fluctuations. For both film heights ξ is suppressed to 0 for $T < T_c$, which is due to the fact that small perturbations decay back to a flat film.[9] The critical temperature T_c is shifted to higher values for increasing film thickness h while the shape of the transition is conserved. This deems plausible as the increasing film-thickness h enlarges the film volume and therefore increases only the bulk free enthalpy of the thin film. This is supported by the determined values for α and β shown in Table I. For both systems α and β are constant inside the error margins for both film thicknesses h. Thereby α is independent of the chosen substrate while β depends on

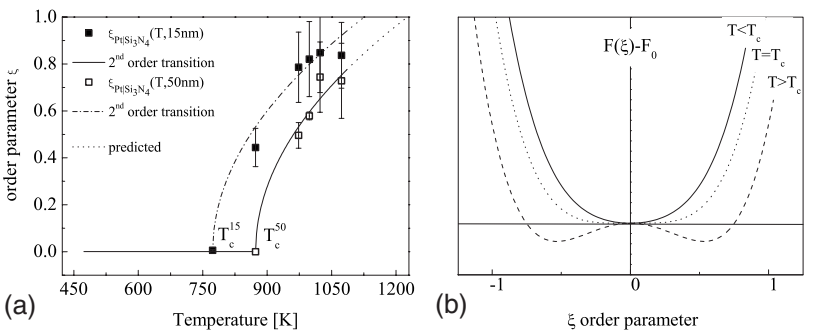

FIG. 5. (a) Order parameter ξ vs temperature T for 15 nm and 50 nm thick Pt films on Si_3N_4 with marked critical temperature T_c. (b) Free energy curves as function of the order parameter ξ of 15-nm-thick Pt on Si_3N_4.

TABLE I. Determined parameters α and β for a continuous-discontinuous second-order transition of Pt/Si_3N_4 and Pt/ZrO_2.

(Metal/substrate)	h (nm)	T_c (K)	α	β
Pt/Si_3N_4	15	773(1)	−0.25(3)	88(7)
Pt/Si_3N_4	50	873(1)	−0.25(3)	88(8)
Pt/ZrO_2	15	914(1)	−0.22(3)	44(6)
Pt/ZrO_2	50	972(1)	−0.22(3)	44(4)

the nature of the substrate and decreases by a factor of 2 comparing the Pt/ZrO_2 with Pt/Si_3N_4 system. Regarding the thermal stability of both systems it can be stated by comparing the critical temperatures T_c that thin-film agglomeration is enhanced on the Si_3N_4 substrate.

The derived parameters α, β, T_c can be implemented in Eq. (2) to obtain the functional shape of the free energy $F(\xi)-F_0$. In Fig. 5(b) the functional shape of the free energy is shown for three temperatures. For $T<T_c$, the free-energy curve exhibits only one minimum, the morphology is stable and continuous, for $T>T_c$ two minima form and the film decomposes in a discontinuous morphology. Hence the found continuous-discontinuous transition of thin-film agglomeration can be treated by the Landau theory and is in agreement with the postulated barrierless nucleation of holes associated to defects by Srolovitz.[9] In conclusion, the nature of the substrate influences significantly the onset of the morphological instabilities and the shape of the free energy.

B. Mechanisms of rupture

In consequence of the previous findings we assume that the rupture mechanism is dominated by nucleation in the spinodal regime.[29] Using the concepts derived in Sec. II B, the experimentally revealed surfaces morphologies obtained by AFM are compared using Minkowski functionals with the prediction of a Gaussian random field. The morphology determined by AFM is shown in Fig. 6(a) and the calculated Minkowski functionals for this morphology in Fig. 6(b). The shapes of the resulting Minkowski functionals show a pronounced resemblance with the expected analytical expressions of a Gaussian random field Eq. (7). In order to test the experimental data on inconsistencies with the model, the effective measures were calculated. A detailed description of this procedure is given by Mecke *et al.*[31,43] In Fig. 6(c), the calculated experimental data is presented alongside the expected behavior of the effective measures in case of a Gaussian random field given by Eq. (8). The experimental data coincide with the model's prediction for film heights h in the vicinity of the average film height $\langle h \rangle$. The fluctuations in the tails between the data and the expected functions for small and large film thicknesses h are a known experimental artifact that contributes to the resolution limits of the AFM image.[44]

Based on this result, the chosen quantitative analysis of the rupture mechanism with Minkowski functionals revealed that the holes are statistically uncorrelated and the hole formation evolves as a Gaussian random field. These characteristics can be attributed to thermal pinning and hole formation by static nucleation barrierless defects such as high energetic triple junctions linking the fa interface with the fs interface, see Fig. 3.

C. Hole growth via surface-limited diffusion

So far it has been shown that the surface evolution during the early stages of thin-film agglomeration can be described by a simple approach for the system's free energy F, see Eq. (2). The next step will focus on the evaluation of the operative mass transport that defines the agglomeration kinetics. Note that agglomeration's thermodynamics and kinetics are methodologically related by Eq. (4). As we intend to apply the Brandon-Bradshaw model to the measured mean hole radius $\langle r \rangle$, it is has to be ensured that the hole radii are normally distributed. In Fig. 7 the hole radius distribution is plotted for a given representative agglomerated sample shown in the inset. The hole radius is normally distributed, in this example with a mean hole radius of $\mu=340$ nm. In comparison to the systematic error due to the resolution limits of image analysis, the obtained standard deviation of σ^2 is of no consequence. Provided that mass is conserved during agglomeration, the Brandon-Bradshaw model can now be applied to determine the surface mass transport coefficient using Eq. (11). The obtained results for D_s of both systems are plotted in Fig. 8(a). For high temperatures, the data is in good agreement with the chosen Arrhenius approach in Eq.

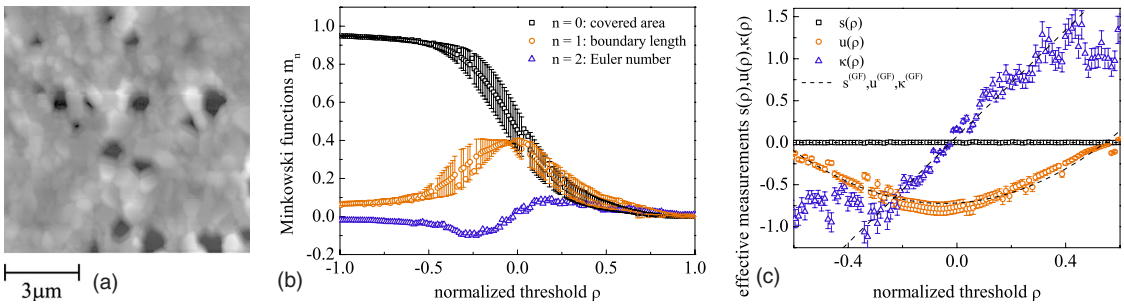

FIG. 6. (Color online) (a) AFM image of agglomeration morphology of Pt on Si_3N_4. (b) The Minkowski functionals, i.e., the normalized area $m_0(h)$, the boundary length $m_1(h)$, and the Euler characteristic $m_3(h)$, as a function of the gray-scale threshold for agglomeration pattern shown in Fig. 3(a). (c) Effective measures $s(h), u(h), \kappa(h)$ according to Eq. (8) which are in good agreement with a Gaussian model (dashed lines).

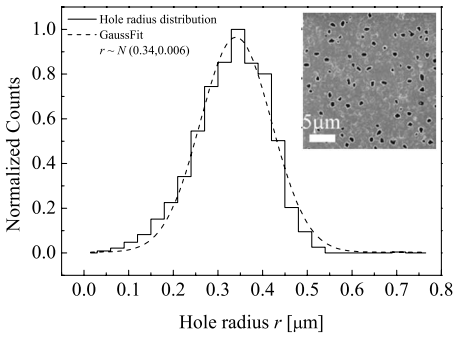

FIG. 7. Plot of the hole radius distribution (solid line) of Pt thin film (50 nm) on Si_3N_4 annealed 986 K for 2 h (inset) and a normal distribution with μ=0.34 μm and σ^2=0.006 (dashed line).

(12a), whereas for lower temperatures T and especially for smaller initial film heights h deviations are visible. Unfortunately the high systematic errors interfere in this region with the results so it cannot be determined whether these deviations are purely statistical or obey a physical reason. To overcome this problem in following works images with higher resolution need to be acquired and merged to conserve the quality of statistical information.

Using Eq. (12a) the activation energy E_a and the prefactor D_0 were calculated from the two slopes and compared with values for Pt self-diffusion from literature [Fig. 8(b)]. The activation energies differ significantly from the literature data but the obtained absolute values for Pt-Pt mass transport on the surface coincide with the velocity regime found in literature. The difference in activation energy E_a between the two chosen substrates is significant. Under the reasonable assumption that the activation energy E_a determined by Bassett *et al.* only contributes to adatom hopping, the substrate-dependent enthalpy of adatom formation E_f has been estimated using Eq. (12b). All experimental results and literature data are summarized in Table II.

In analogy to Gontier-Moya *et al.*,[17] we conclude from Fig. 8 that in comparison to a Pt-Pt system (i.e., Blakely[59]) the interaction of Pt atoms with a dielectric substrate alters E_f and therefore the adatom concentration and the mobility. As the Brandon-Bradshaw model disregards any involvement of the fs interface, the determined activation energies E_a for mass transport have to be treated as a first approximation. In order to overcome the model's shortcomings, two experimental strategies are presented in the next section and are used to clarify the impact of the film-substrate interface on the agglomeration kinetics.

D. Interfacial energies and adhesion

In order to determine the velocity of the agglomeration at the fa and the fs interface separately, annealed samples of reasonable thickness were analyzed via FIB nanotomography.[60] The choice of a larger film thickness is necessary to minimize the interaction between the processes at the two interfaces. In Fig. 9(a), a reconstructed 180-nm-thick Pt thin film on Si_3N_4 acquired by FIB nanotomography is shown. The film was annealed at T_a=986 K for 2 h. Analysis of the fa interface Fig. 9(b) revealed a strong faceted surface topography with randomly distributed holes, λ_{fa}=0.05. The fs interface shown in Fig. 9(c) has been laid open by cropping the data set in z direction up to two voxel layers. The fs interface is strongly agglomerated and uncovered by approximately one half, λ_{fs}=0.45. That means compared to the fa interface an increase by a factor of 9, the equally analyzed Pt/ZrO_2-system exhibited a factor of only 2. Hence the velocity of the agglomeration kinetics differs significantly depending on the nature and the properties of the interfaces. In the case of the Pt/Si_3N_4, the ca-interface accelerates agglomeration to such an extent that the agglomeration regimes at the fa interface and fs interface differ. This can arise from weak adhesion as well as from relaxation processes such as dislocation core spreading.

To evaluate the impact of adhesion on the agglomeration kinetics, the interfacial energies of the two systems are determined. For this purpose samples are used that have already formed facetted islands, so that the Wulff-Kaishew theorem Eq. (14) can be applied to measure the interfacial energy. The orientation of the particles were confirmed to be [111] texturized by x-ray diffraction measurements.

The samples have been analyzed by means of FIB nanotomography. In Fig. 10(a), a reconstructed Pt island on Si_3N_4 is shown. A cut through the mass center of the island is extracted and plotted in Fig. 10(b). Using standard image-analysis techniques the truncation depth Δh_s and the orienta-

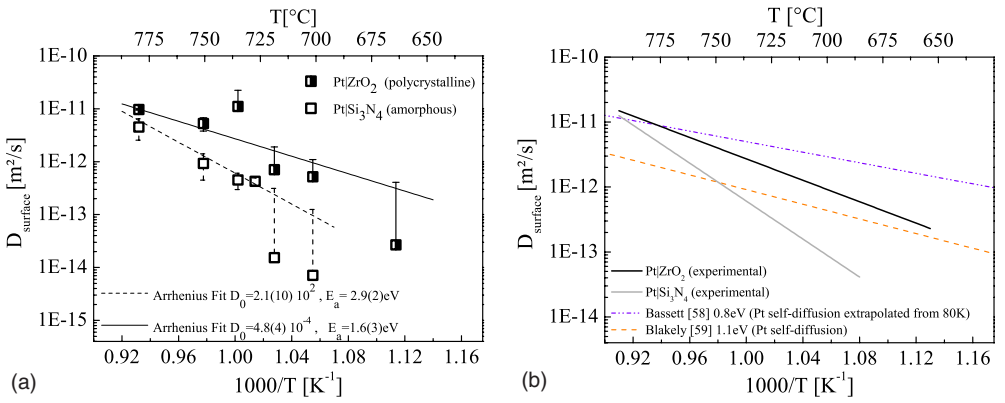

FIG. 8. (Color online) (a) Platinum surface self-diffusion coefficients as derived from the Brandon-Bradshaw model and (b) comparison of measured surface self-diffusion coefficients with literature data of Pt surface self-diffusion (Refs. 58 and 59).

TABLE II. Values for surface self-diffusion of Pt on Pt.

	Surface self-diffusion (Pt/Pt)				
(Metal/substrate)	Temperature range (K)	D_0 (m^2/s)	E_s (eV)	E_f (eV)	Ref.
(Pt/Si_3N_4)	948–1073	$2.5(10)\times10^2$	2.9(2)	2.1(2)[a]	This work
(Pt/ZrO_2)	898–1073	$4.8(4)\times10^{-4}$	1.6(3)	0.8(3)[a]	This work
(Pt foil)[b]	673–1273	4.0×10^{-7}	1.12		59
(Pt/Pt)[c]	80–120	5.7×10^{-8}	0.80		58

[a]Calculated using adatom migration energy of Ref. 58.
[b]Surface self-diffusion measured by interference microscopy.
[c]Adatom migration measured by field ion microscopy.

tion θ_{hkl} of the crystal's facets are determined. The same procedure based on Fig. 10(c) is applied to SEM cross sections of the disintegrated films of both systems. These measurements result in a value for the adhesion energies E_{ad} of the two systems. For Pt on Si_3N_4 an adhesion energy of $E_{ad}=0.9(2)$ J/m^2 is achieved, in case of Pt/ZrO_2 the adhesion energy is $E_{ad}=1.2(2)$ J/m^2. All obtained values are shown in Table III. The measured values show a reasonable agreement with literature data[61] for the similar Pt/Al_2O_3 system with an adhesion energy of $E_{ad}=1.05(8)$ J/m^2. The presented results are in accordance with the established theory that the adhesion of a crystalline metal on an amorphous substrate is generally smaller than in the case of an crystalline substrate.[35,37] In analogy to Ref. 62, the enhanced agglomeration kinetics at the fs interface can be attributed to the low adhesion energy in comparison to the surface energy of Pt,[63] i.e., $\gamma_{s,111}=1.7$ J/m^2. The crystalline-amorphous Pt/Si_3N_4 interface with a lower adhesion energy than the crystalline-crystalline Pt/ZrO_2 interface shows a distinctly enhanced hole formation at the fs interface. The general experimental result, that a low adhesion energy enhances the film instability, is in agreement with the predicted impact of the contact angle on the linear stability of a catenoidal hole found by numerical calculations.[27] But the difference in adhesion energy cannot only be responsible for the large deviation of agglomeration velocities at the fa interface and fs interface, respectively. Regarding the work of Dornel *et al.*[18] an impact of surface anisotropies on the kinetics can be excluded. Therefore, the impact of the lattice mismatch and the evolving stresses at the fs interface on the film morphology is studied in more detail in an upcoming work.

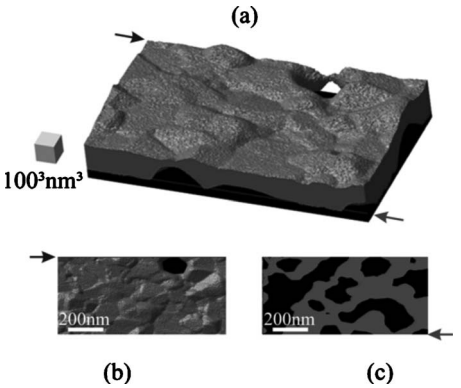

FIG. 9. (a) Three-dimensional (3D) reconstruction of an agglomerated 180-nm-thick Pt film on Si_3N_4 obtained via FIB nanotomography with associated top views on (b) the Pt/ambient interface and (c) the Pt/Si_3N_4 interface.

V. CONCLUSIONS

In essence it has been shown that thin-film agglomeration under the point of view of basic thermodynamics can be phenomenologically described by nucleation in the spinodal regime using a common Landau ansatz. The functional shape of the free energy for the Pt/Si_3N_4 system and the Pt/ZrO_2

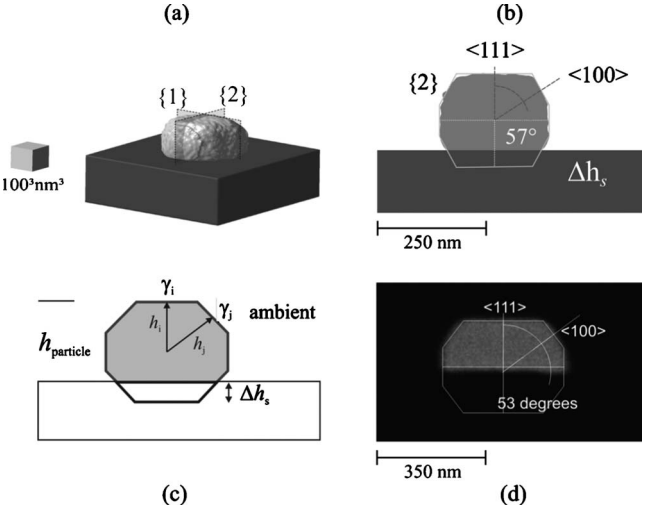

FIG. 10. (a) 3D reconstruction of a facetted Pt particle on a Si_3N_4 substrate with cross sections {1}{2} through particle's mass center obtained by FIB nanotomography. (b) Cross section {2} of reconstructed Pt particle and fitting Wulff-Construction of the particle with indicated truncation depth Δh_s. (c) Schematic illustration of the Wulff-Construction of an isolated particle on a random substrate and necessary measurands to determine the adhesion energy E_{ad}. (d) SEM image of FIB-etched Pt particle and apparent Wulff-Construction.

TABLE III. Measured adhesion energies E_{ad} of Pt/Si_3N_4, Pt/ZrO_2 and literature data for Pt/Al_2O_3.

(Metal/substrate)	θ_{hkl}	E_{ad} (J/m^2)	Ref.
Pt/Si_3N_4	54(3)	0.9(2)[a]	This work
Pt/ZrO_2	42(3)	1.2(2)[a]	This work
Pt/Al_2O_3		1.05(8)[b]	61

[a]Calculated using surface energies of Ref. 63.
[b]Calculated from the dihedral angle.

system has been derived, thereby a different substrate material leads to a significant change in the critical temperature T_c and in the β value. The nature of α and β is subjected to further research. On closer inspection it can be seen that T_c is shifted to higher temperatures for equal h of the two systems, which means that the thin-film stability in the presence of a *crystalline/crystalline* interface is increased compared to *crystalline/amorphous* interface. This is remarkable regarding the large lattice misfit f between Pt and ZrO_2. These findings are substantiated by the surface morphology analysis with Minkowski functionals that clearly indicates that the mechanism of rupture is based on defect-induced barrierless nucleation of holes. Obviously a rupture mechanism that is dominated by barrierless nucleation needs to be a second-order transition in inference. Since recent results have shown, that at constant coverage ξ the contour length increases with decreasing film thickness h, further morphological studies with Minkowski functionals are planned. The analysis of multiple cross sections prepared by FIB etching revealed quantitatively that independent from the substrate and thickness, hole formation occurs predominantly in presence of triple lines. The coupled morphology-growth mechanism study with the model of Brandon-Bradshaw enabled to determine the Pt-Pt surface mass transport coefficients which are in good agreement with literature data. Nanotomography of the rupturing thin film show an accelerated rupturing at the crystalline/amorphous interface, which explains the differing formation enthalpies E_f determined via the Brandon-Bradshaw model and support the common hypothesis that nature of the present interfaces has a significant impact on the agglomeration mechanism. Combined with the determined adhesion energies E_{ad} 0.9(2) J/m^2 for Pt/Si_3N_4 and 1.2(2) J/m^2 for Pt/ZrO_2, experimental evidence is found that in a case of a crystalline/amorphous interface the adhesion is reduced and agglomeration kinetics is accelerated. It is shown that two in general independent physical processes control the morphological evolution and kinetics of thin-film agglomeration: one attributes to the film-ambient interface and the other to the film-substrate interface. Depending on the ratio between surface and adhesion energy, the agglomeration kinetics at the film-substrate interface can be enhanced up to a factor of 9, which requires the presence of fast diffusive pathways inside the deposited film. The presence of a fast diffusive pathway is inevitably combined with a second diffusion mechanism, most likely triple junction diffusion, that contributes to the kinetics of thin-film agglomeration.

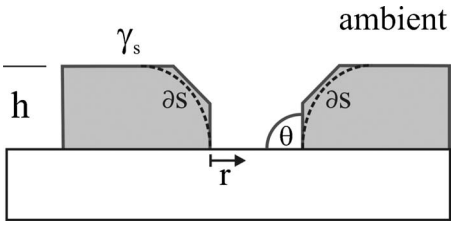

FIG. 11. Schematic illustration of the hole formation according to the Brandon-Bradshaw model.

ACKNOWLEDGMENTS

The authors wish to acknowledge the financial supported by the Swiss Bundesamt für Energie (BfE), Swiss Electric Research (SER), Competence Center of Energy and Mobility (CCEM), and Swiss National Foundation (SNF) and would like to thank the EMEZ (Electron Microscopy Center, ETH Zurich) for their support. In addition Henning Galinski thanks Ralph Spolenak, Iwan Schenker, Joakim Reuteler, and Anna Evans for fruitful and stimulating discussions.

APPENDIX: VALIDITY OF THE BRANDON-BRADSHAW MODEL

For describing structural changes in thin films due to diffusion processes, Brandon and Bradshaw[14,15] used the grain-boundary grooving model from Mullins and tried to adapt it to growing holes in the films. The aim of the following calculation is to associate geometrical properties of the sample such as average hole radius r and film thickness h with the surface-diffusion coefficient of the film material. The used model is based on following assumptions, see also Fig. 11: (1) the contact angle Θ as shown in figure is 90°. (2) The cross section of the rim is circular. (3) Surface diffusion is dominant. (4) The surface free energy γ_s is constant. (5) The holes are circular. (6) The substrate does not influence the process.

The flow of surface atoms is due to the difference in chemical potential in regions of different curvature as seen earlier by Mullins. The net flux j_s of atoms along the surface is

$$j_s = -\frac{D_s}{kT}\frac{\partial \mu}{\partial s}\nu, \tag{A1}$$

where s is the distance along the rims surface. Since γ_s is considered constant, the pressure difference across the surface is $\gamma_s(\frac{1}{x}-\frac{1}{r})$ and the difference in chemical potential is

$$\mu_L - \mu_\infty = -\Omega\gamma_s\left(\frac{1}{x}-\frac{1}{r}\right) = -\Omega\gamma_s/x; \quad r \gg x, \tag{A2}$$

where the subscript L refers to equilibrium with the local surface and ∞ with a flat surface, assuming that the curvature changes from $\frac{1}{x}$ to zero within a distance πx. Inserting $\partial s = \pi x$ and $\partial\mu = -\Omega\gamma_s/x$ into Eq. (A1) one obtains

$$j_s = \frac{D_s\Omega\gamma_s}{kT\pi x^2}\nu. \tag{A3}$$

The total perimeter across which diffusion occurs is $2\pi r$ resulting in a volume rate of transfer of materials (dV/dt) by surface diffusion equal to $j_s 2\pi r\Omega$. Substituting this into Eq. (A3) leads to

$$\frac{dV}{dt} = \frac{2D_s\Omega^2\gamma_s r}{kTx^2}\nu. \tag{A4}$$

In order to maintain constant volume of film material, the following equations have to be fulfilled:

$$2\pi r\frac{\pi x^2}{2} = \pi r^2 h, \tag{A5}$$

$$\pi x^2 = rh. \tag{A6}$$

Substituting this into Eq. (A4) reads

$$\frac{dV}{dt} = \frac{2D_s\Omega^2\gamma_s\pi}{kTh}\nu. \tag{A7}$$

Using the geometrical relation $dV=2\pi rx\,dr$ and Eq. (A6) it follows that

$$\frac{dV}{dt} = 2\pi r\sqrt{\frac{rh}{\pi}}\frac{dr}{dt} \tag{A8}$$

and by substituting dV/dt using Eqs. (A7) and (A8) one gets

$$\frac{dr}{dt} = \frac{D_s\Omega^2\gamma_s\nu}{\pi kThr}\sqrt{\frac{\pi}{rh}} = \frac{Br^{-3/2}\pi^{1/2}}{h^{3/2}}. \tag{A9}$$

Integration finally gives

$$r^{5/2} = \frac{5\pi^{1/2}Bt}{2h^{3/2}} \tag{A10}$$

and the dependency of the surface-diffusion coefficient D_s on geometrical parameters such as hole radius r and film thickness h. Jiran and Thompson have proposed a different model[6] that adepts to the morphological evolution and void growth found experimentally for fingering instabilities.[19] Jiran and Thompson predict that the hole radius r scales linear with time t and depends inverse cubic on the film height h,

$$r = \frac{2D_0\Omega^2\gamma_s\exp[-E_a/k_bT]}{kT\pi h^3}. \tag{A11}$$

The thickness dependence of the hole radius r is determined from the slope n of the fitted lines in Fig. 12. The fitted slopes n for each substrate and temperature are in the same range as predicted by the Brandon-Bradshaw model with $n_{BB}=-\frac{3}{5}$. The scaling behavior of the Jiran-Thompson model with a slope of $n_{JT}=-3$ cannot be reproduced. The observed discrepancy between the model of Jiran-Thompson and the experimental data set of this work can be explained by the different experimental conditions. In the work of Jiran and Thompson the perturbation are not associated to static polycrystalline defects such as triple junctions but to the free surface of the line edge of the deposited metal strip. By changing the type of initial perturbation one certainly changes the mechanism of rupture, its kinetics, and hence the boundary conditions of thin-film agglomeration.

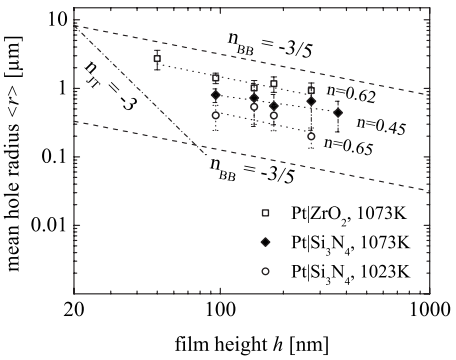

FIG. 12. Log-log graph of the mean hole radius r as function of the film height h. Fitted slopes n are shown for data with differing temperature and substrate, the predicted slopes for the Brandon-Bradshaw model $n_{BB}=-\frac{3}{5}$ and the model by Jiran and Thompson $n_{JT}=-3$ are plotted.

The model of Brandon and Bradshaw has been extended by Srolovitz,[10] whereby the hole evolution is considered to be impacted either by surface-diffusion kinetics or by evaporation-condensation kinetics. The growth rate for surface-diffusion kinetics is given by

$$\frac{dr}{dt} = VB^{1/4}t^{-3/4}\{\ln^3[Bt(h/\tan\theta)^4] + \cdots\}, \tag{A12}$$

where V is a free fitting parameter. The model considers the influence of the substrate by taking into account the wetting angle θ. It is reported that the critical ratio $h/\tan\theta$ of the film thickness h and the wetting angle θ triggers the hole growth.[10] Unfortunately this model attributes to the dynamics of thin-film agglomeration and is not applicable to the present isochronical data set.

*henning.galinski@mat.ethz.ch

[1] Z. Suo, Int. J. Solids Struct. **37**, 367 (2000).
[2] J. R. Lloyd, J. Phys. D: Appl. Phys. **32**, R109 (1999).
[3] R. Kirchheim, Acta Metall. Mater. **40**, 309 (1992).
[4] F. B. P. X. Jiang, H. Huang, and S. F. Bent, Chem. Mater. **20**, 3897 (2008).
[5] D. J. Srolovitz and M. G. Goldiner, JOM **47**, 31 (1995).
[6] E. Jiran and C. V. Thompson, J. Electron. Mater. **19**, 1153 (1990).
[7] M. W. Finnis, J. Phys.: Condens. Matter **8**, 5811 (1996).
[8] J. T. M. D. Hosson and B. J. Kooi, Surf. Interface Anal. **31**, 637 (2001).
[9] D. J. Srolovitz and S. A. Safran, J. Appl. Phys. **60**, 247 (1986).
[10] D. J. Srolovitz and S. A. Safran, J. Appl. Phys. **60**, 255 (1986).

[11] F. Génin, W. Mullins, and P. Wynblatt, Acta Metall. Mater. **40**, 3239 (1992).
[12] F. Génin, W. Mullins, and P. Wynblatt, Acta Metall. Mater. **42**, 1489 (1994).
[13] C. Stöcker and A. Voigt, Proceedings of the Fifth Workshop on Modeling in Crystal Growth, IWMCG-5 [J. Cryst. Growth **303**, 90 (2007)].
[14] R. Brandon and F. Bradshaw, Technical Report, Royal Aircraft Establishment Farnborough, England, p. 38, 1966.
[15] F. Bradshaw, R. Brandon, and C. Wheeler, Acta Metall. **12**, 1057 (1964).
[16] I. Beszeda, I. Szabo, and E. Gontier-Moya, Appl. Phys. A: Mater. Sci. Process. **78**, 1079 (2004).
[17] E. G. Gontier-Moya, I. Beszeda, and F. Moya, Proceedings of the 22nd European Conference on Surface Science [Surf. Sci. **566-568**, 148 (2004)].
[18] E. Dornel, J.-C. Barbé, F. de Crécy, G. Lacolle, and J. Eymery, Phys. Rev. B **73**, 115427 (2006).
[19] E. Jiran and C. Thompson, Thin Solid Films **208**, 23 (1992).
[20] W. Kan and H. Wong, J. Appl. Phys. **97**, 043515 (2005).
[21] C. Kennefick and R. Raj, Acta Metall. **37**, 2947 (1989).
[22] E. Shaffir, I. Riess, and W. Kaplan, Acta Mater. **57**, 248 (2009).
[23] A. Gladkikh, Y. Lereah, E. Glickman, M. Karpovski, A. Palevski, and J. Schubert, Appl. Phys. Lett. **66**, 1214 (1995).
[24] S. Sharma and J. Spitz, Thin Solid Films **65**, 339 (1980).
[25] H. Wong, P. W. Voorhees, M. J. Miksis, and S. H. Davis, Acta Mater. **48**, 1719 (2000).
[26] H. Wong, M. J. Miksis, P. W. Voorhees, and S. H. Davis, Acta Mater. **45**, 2477 (1997).
[27] H. Wong, P. W. Voorhees, M. J. Miksis, and S. H. Davis, J. Appl. Phys. **81**, 6091 (1997).
[28] M. S. McCallum, P. W. Voorhees, M. J. Miksis, S. H. Davis, and H. Wong, J. Appl. Phys. **79**, 7604 (1996).
[29] U. Thiele, M. G. Velarde, and K. Neuffer, Phys. Rev. Lett. **87**, 016104 (2001).
[30] U. Thiele, Eur. Phys. J. E **12**, 409 (2003).
[31] J. Becker, G. Grun, R. Seemann, H. Mantz, K. Jacobs, K. R. Mecke, and R. Blossey, Nature Mater. **2**, 59 (2003).
[32] K. Jacobs, R. Seemann, and K. Mecke, *Statistical Physics and Spatial Statistics* (Springer, Berlin, 2000), pp. 72–91.
[33] Y. Mao, T. McLeish, P. Teixeira, and D. Read, Eur. Phys. J. E **6**, 69 (2001).
[34] S. Herminghaus, K. Jacobs, K. Mecke, J. Bischof, A. Fery, M. Ibn-Elhaj, and S. Schlagowski, Science **282**, 916 (1998).
[35] L. P. H. Jeurgens, W. G. Sloof, F. D. Tichelaar, and E. J. Mittemeijer, Phys. Rev. B **62**, 4707 (2000).
[36] R. Benedictus, A. Böttger, and E. J. Mittemeijer, Phys. Rev. B **54**, 9109 (1996).
[37] F. Reichel, L. P. H. Jeurgens, and E. J. Mittemeijer, Phys. Rev. B **74**, 144103 (2006).
[38] G. Renaud, P. Guénard, and A. Barbier, Phys. Rev. B **58**, 7310 (1998).
[39] E. Mutoro, B. Luerssen, S. Günther, and J. Janek, Solid State Ionics **179**, 1214 (2008).
[40] A. Novick-Cohen, J. Stat. Phys. **38**, 707 (1985).
[41] L. Landau, Zh. Eksp. Teor. Fiz. **7**, 627 (1937); see *Collected Papers of L. D. Landau* (Pergamon, London, 1973), pp. 193 and 209.
[42] S. P. Baker, L. Zhang, and H. Gao, J. Mater. Res. **17**, 1808 (2002).
[43] H. Mantz, K. Jacobs, and K. Mecke, J. Stat. Mech.: Theory Exp. 2008, P12015.
[44] J. Schmähling and F. Hamprecht, Wear **262**, 1360 (2007).
[45] R. J. Adler and D. Firman, Philos. Trans. R. Soc. London, Ser. A **303**, 433 (1981).
[46] K. R. Mecke, Acta Phys. Pol. B **28**, 1747 (1997).
[47] G. S. Grest and D. J. Srolovitz, Phys. Rev. B **30**, 6535 (1984).
[48] W. W. Mullins, J. Appl. Phys. **28**, 333 (1957).
[49] H. P. Bonze, Crit. Rev. Solid State Mater. Sci. **6**, 171 (1976).
[50] G. Wulff, Z. Kristallogr. **34**, 449 (1901).
[51] C. Herring, Phys. Rev. **82**, 87 (1951).
[52] R. Kaishew, Bull. Acad. Sc. Bulg. (Ser. Phys.) **2**, 191 (1951).
[53] P. Müller and R. Kern, Appl. Surf. Sci. **164**, 68 (2000).
[54] F.-H. Lu, M. L. Newhouse, R. Dieckmann, and J. Xue, Solid State Ionics **75**, 187 (1995) interfaces in Ionic Materials.
[55] P. Thévenaz, U. Ruttimann, and M. Unser, IEEE Trans. Image Process. **7**, 27 (1998).
[56] C. M. Müller, F. C. F. Mornaghini, and R. Spolenak, Nanotechnology **19**, 485306 (2008).
[57] J. W. Cahn, J. Chem. Phys. **42**, 93 (1965).
[58] D. Bassett and P. Webber, Surf. Sci. **70**, 520 (1978).
[59] J. Blakely and H. Mykura, Acta Metall. **10**, 565 (1962).
[60] L. Holzer, F. Indutnyi, P. Gasser, B. Münch, and M. Wegmann, J. Microsc. **216**, 84 (2004).
[61] M. McLean and E. D. Hondros, J. Mater. Sci. **6**, 19 (1971).
[62] T. Nolan, R. Beyers, and R. Sinclair, MRS Symposia Proceedings No. 202 (Materials Research Society, Pittsburgh, 1991), p. 95.
[63] J.-M. Zhanga, F. Ma, and K.-W. Xu Appl. Surf. Sci. **229**, 34 (2004).